Integrative Bioscience Nexus

Biologica Aid

Article

Efficient Removal of Paraquat by *Rhizobium* sp. Strain HRI101-4: A Combined Affirmation Through In Vitro and *In Silico* Studies

Jui Biswas[1], Shirmin Islam[1], Suvro Biswas[1], Md. Ariful Islam[1], Mohammad Abdullah Taher[2], Pranab Karmaker[2], Md. Salah Uddin[1], Shahriar Zaman[1], Md. Abu Saleh[1,*]

[1]Microbiology Laboratory, Department of Genetic Engineering and Biotechnology, University of Rajshahi, Rajshahi-6205, Bangladesh
[2]Bangladesh Reference Institute for Chemical Measurements (BRiCM), Dr. Qudrat-i-Khuda Road, Dhaka-1205, Bangladesh
* Correspondence: Md. Abu Saleh (saleh@ru.ac.bd)

Abstract: Soil microorganisms can respond to herbicides after exposure, with certain bacteria capable of breaking them down and using the energy for growth. Herbicides like paraquat (C12H14Cl2N2), which inhibit plant photosynthesis, pose significant environmental and health risks. In this study, an herbicide-degrading Rhizobacterium was isolated from agricultural soil treated with paraquat. The strain was identified through morphological and molecular techniques, and its growth was optimized at 35℃ over 72 hours, with pH levels of 7 and 7.5. Spectrophotometric and HPLC analyses revealed 99% paraquat degradation, reducing the concentration to 8.82 µg/ml, with optimal degradation occurring at pH 4 and 30℃. The strain also demonstrated tolerance to certain heavy metals and resistance to various antibiotics. 16S rRNA sequencing confirmed a 98% similarity to Rhizobium sp. strain HRI101-4, emphasizing its potential in mitigating paraquat pollution. Molecular docking analysis was conducted to explore the binding interactions between five enzymes from Rhizobium sp. The binding affinities, indicated by docking scores, ranged from -7.3 for dehydrogenase to -5.2 for malate dehydrogenase. The analysis showed that enzymes from Rhizobium sp. interact with paraquat in distinct manners, suggesting a variety of binding affinities and interaction sites. This indicates that these enzymes may influence paraquat's functions, potentially affecting its degradation activity.

Keywords: *Rhizobium*, Paraquat, Degradation, HPLC, *In silico* analysis

Academic Editor: Dr. Hamed Hamuoda

Received: 2 May 2026
Revised: 12 June 2026
Accepted: 15 June 2026
Published: 05 July 2026

1. Introduction

In the era of agriculture, soil is one of the most crucial components of the ecosystem and is also susceptible to contamination because it can be easily contaminated through herbicides or pesticides. The application of herbicides in agricultural field can change the normal conditions of microorganisms which may induce the fertility of soil [1]. Herbicides interact with soil microorganisms, when they are administered in agricultural settings. As agriculture's reliance on herbicides and pesticides grows, so does the concern about their damaging effects on soil microorganisms, which play a vital role in both our agricultural sector and our ecology. Herbicides should be tested for increased toxicity as soon as possible after application [1]. Furthermore, the exertion of herbicides in the agricultural field is responsible for increasing the amount of herbicides in the top layer of soil, which may be toxic for the next year's growing crops and also responsible for inducing new genotypes that are weed-resistant [2].

Whereas herbicides may be useful for controlling unwanted plants in the crop field, the long-term use of herbicides is not preferable [3].

Paraquat, whose trade name is paraquat, is widely used as a non-selective and broad-spectrum herbicide. It is also known as a quaternary ammonium bipyridyl compound (1, 1'-dimethyl-4, 4' bipyridylium dichloride) [4]. Paraquat has been described as a chemical flamegun that kills plant parts above the ground without harming the roots. These actions mostly destroy annual weeds, but deeper-rooted and rhizomatous weeds will sprout. It is a hypersensitive herbicide that operates inside the chloroplast, converting photosystem-I (PSI) into electrons. Paraquat receives a single electron to form a stable reduced cation radical. It interacts quickly with dioxygen to produce superoxide and catalyzes the creation of superoxide. Superoxide is derived from water through photosynthetic electron transport. Superoxide dismutase (SOD), a chloroplast superoxide dismutase, reacts with superoxide ions and cycles between Fe^{2+} and Fe^{3+} to create hydroxy radicals. This is achieved through the intermediacy of free iron peroxide [5].

Paraquat is mostly absorbed by soil for its ionic properties and for prolonging the chemical structure of the soil. The presence of carboxylic and phenolic compounds in clay's organic matter enhances paraquat adsorption via cation exchange. Furthermore, paraquat can be gradually dissolved by a variety of microorganisms or by breakdown mechanisms such as hydrolysis, making it virtually invisible in both water and land environments [6]. Paraquat poisoning is a significant issue for both the environment and public health in Asia [7]. Additionally, the use of herbicides contaminates soil and water, which in turn contaminates agricultural products and food items, posing a risk to human health and having negative consequences for the environment and public health [2]. Accepting the hazardous effects of paraquat residues on the environment and humans, research on microorganisms that can digest paraquat is necessary. Microorganisms such as fungi, bacteria, and yeast play an important role in the degradation of paraquat [4]. Bio-transformation of herbicides is carried out by several microorganisms and herbicides that continue to exist or occur over a prolonged period can also be broken down through herbicides-degrading microorganisms such as bacteria and fungi, which utilize them as a source of nutrients and energy [8].

For the degradation of paraquat, a number of oxidoreductive enzymes have been investigated, including ferredoxin reductase, dihydroxy acid dehydratase, and VirB8 [9,10]. In order to maximize the importance and interaction of protein ligands, molecular docking and simulation are practical and affordable ways [11]. In Bangladesh, various pre- and post-emergence herbicides like paraquat are widely used for controlling broadleaf weeds in leguminous crops. This herbicide causes severe environmental pollution. The protection of the environment has become a major issue globally for the well-being of the people and economic development. Herbicide biodegradation by existing nitrogen-fixing bacteria in root nodules and the rhizosphere has gained attention among scientists. In the current work, *Rhizobium* sp., a type of bacteria that breaks down herbicides, was isolated, recognized, and optimized from an agricultural area. After that, the commonly used herbicide paraquat was subjected to bioremediation using enzymes from *Rhizobium* sp. for herbicide degradation. It provides an innovative, economical approach for reducing herbicide toxicity by identifying and improving *Rhizobium* sp. for paraquat breakdown and using molecular docking to investigate important oxidoreductive enzymes. This study, which was carried out in Bangladesh, where paraquat use is common, emphasizes how *Rhizobium* sp. plays a dual role in improving soil fertility and degrading herbicides, offering scalable alternatives for environmentally friendly farming practices and sustainable agriculture.

The aim of the investigation was to establish a successful bioremediation plan for paraquat, with an emphasis on the isolation and improvement of *Rhizobium* sp., a nitrogen-fixing bacteria that has the ability to both degrade herbicides and improve soil fertility. Additionally, using molecular docking to investigate key oxidoreductive enzymes in order to unravel the metabolic mechanisms underlying paraquat degradation.

2. Materials and Methods

In order to study nitrogen-fixing bacteria, soil samples were gathered on Jun 2, 2022, from the legume crop (*Phaseolus vulgaris* L.) field located in Katakhali a district of Rajshahi (Latitude: 24.363685N, Longitute: 88.649201E). These samples were carefully placed in polythene bags and subsequently transported to the laboratory. Additionally, the herbicide, paraquat ($C_{12}H_{14}Cl_2N_2$: 1,1'-Dimethyl-4,4'-bipyridinium dichloride) was obtained from the local market and stored within the laboratory.

2.1. Chemicals used

The paraquat used was a commercial paraquat (containing 276 g active ingredient/L of paraquat), bought from a local store in Katakhali, Rajshahi. To evaluate the tolerance or resistance of bacterial strains by the use of paraquat as a sole source of carbon, a YEMA without a carbon source is used. The composition of the medium (pH 7.0-7.2) was as follows:

Manitol (10 g/L), KH_2PO_4 (.5 g/L), $MgSO_4$ $7H_2O$ (0.2 g/L), Yeast extracts (0.5 g/L), NaCl (0.10 g/L), Agar (10 g/L). The media was supplemented with paraquat and were used to test the tolerance or resistance of the one strain to Paraquat.

2.2. Bacteria strains

A single bacterial strain was selected to test its tolerance and degrading ability to paraquat. The strain was originally isolated from legume crop cultivated in an agricultural field situated in Katakhali, Rajshahi. The selection was based on the strain's nitrogen-fixing ability, which is a characteristic of rhizobia. To isolate the strain, soil samples were collected from the root zone of leguminous plants, and serial dilutions of the soil were plated onto Yeast Extract Mannitol Agar (YEMA) medium. The plates were incubated at 28°C for 48-72 hours. Nitrogen-fixing colonies were identified by their characteristic growth and ability to form nodules on leguminous plants. The selection of the strain was based on its ability to fix nitrogen. The selected strain is *Rhizobium* sp.

2.3 Preparation of inoculum

For preparing the inoculum, soil was collected from the legume crops field in Katakhali, Rajshahi. After collecting the soil, we filtered it through filter paper and then inoculated it in LB liquid media containing 5.52 mg/ml of paraquat. Finally, it was incubated for 16-18 hours at a temperature of 37 °C to prepare a mixed bacterial culture.

2.4 Enrichment and isolation of paraquat-degrading bacterium

A paraquat-degrading bacterium was isolated from the soil sample (which had likely been treated with paraquat for almost 5 years to control unwanted plants) using LB agar media with various concentrations of paraquat. Paraquat was used as a source of nutrients and energy for bacterial growth. After 36 hours of shaking, bacterial growth was observed in the media containing paraquat, indicating that the bacteria present in the collected soil sample were capable of metabolizing the herbicide. The isolation process was carried out as follows: one gram of paraquat-treated soil sample was suspended in 250 ml Erlenmeyer flasks containing 100 ml of LB liquid media. Control flasks without an inoculum were also prepared to account for any abiotic disappearance of paraquat. The primary enrichment was shaken at 120 rpm for up to 3 days on an orbital shaker. When the cultures reached adequate turbidity, they were used as a source of inoculum in subsequent experiments. After that, the enrichment culture was streaked onto LB agar media supplemented with various concentrations (2.76 μg/ml, 5.52 μg/ml, and 8.82μg/ml) of paraquat and incubated at 37 °C for 36 hours. Colonies were then isolated and sub cultured for the present work.

2.5 Biochemical, and physiological characterization of the isolate

The biochemical characterization of the isolate was performed to check the purity of the nitrogen-fixing bacteria by adding Congo red to the YEMA media. Physiological characterization of the isolate was conducted by measuring the absorbance at 290 nm OD in an enriched medium with paraquat to determine the optimum temperature and pH at which the isolate can effectively degrade paraquat. The isolated bacteria were grown at different pH levels (4-7) and temperatures (25°C, 30°C, 37°C, and 40°C) to identify the most favorable growth conditions.

2.5.1 Antibiotic sensitivity tests of the isolates

Mueller-Hinton agar plates were used to assess the isolated bacterium's sensitivity to antibiotics using the disc diffusion method. Antibiotic discs containing penicillin, amoxicillin, gentamicin, ciprofloxacin, ampicillin, kanamycin, chloramphenicol, doxycycline, and erythromycin were prepared by spreading a bacterial suspension (0.5 McFarland standard) on the agar. The plates were incubated for 18 to 24 hours at 37°C. The sensitivity or resistance of the bacterium was then evaluated by measuring and comparing the inhibition zones surrounding the discs to CLSI criteria, which revealed information about its antimicrobial profile [12].

2.5.2 Heavy metal resistance profile

The selected strain was tested for its resistance to various heavy metals, including lead nitrate ($Pb(NO_3)_2$), cadmium chloride ($CdCl_2$), copper chloride ($CuCl_2$), sodium arsenite ($NaAsO_2$), and mercury iodide (HgI_2). Stock solutions of these heavy metals were prepared at concentrations of 2, 4, 6, 8, and 10 nM. The bacterium was exposed to these concentrations to assess its tolerance and resistance capabilities. This method helps evaluate the strain's ability to withstand and potentially detoxify harmful heavy metal ions, providing insight into its resilience in polluted environments.

2.5.3 Salt tolerance test

The test was performed using 2% NaCl in YEMA basal medium to evaluate the growth of the isolate. Certain rhizobial isolates are sensitive to high salt concentrations, and the presence of 2% NaCl helps assess their growth inhibition, which is valuable for identifying the antioxidant capacity of intact cells. This method is also effective for isolating salt-tolerant bacteria, as those capable of surviving and growing in this saline environment are classified as salt-tolerant strains.

The ability to thrive in high-salt conditions indicates the bacterium's resilience and potential for applications in saline environments.

2.5.4 Antioxidant capacity of intact cells

Intact cells were prepared by centrifuging a freshly prepared broth culture at 10,000 rpm for 10 minutes after incubating for 24 hours. The resulting cell pellet was resuspended, and the cell density was adjusted to 10^8 CFU/ml using a 0.85% saline solution and the McFarland 0.5 standard. The optical density (OD) of the cell suspension was then measured using a GENSYS 10S UV-VIS Thermo Scientific spectrophotometer. To determine the antioxidant activity, an equation was applied to calculate the percentage of antioxidant scavenging. The scavenging rate of SNKUII was calculated using the following formula: Scavenging rate of SNKUII (%) = [1-(0.396-0)/0.282]X100%.

2.5.5 Screening of hemolytic activity

Rhizobium bacterial cultures were grown overnight in appropriate liquid medium and then streaked onto Nutrient Agar (NA) plates supplemented with 4% sheep blood agar base (HiMedia Laboratories, Mumbai, India). The plates were incubated at 37°C for 48 hours. After incubation, the presence or absence of hydrolysis zones around the bacterial colonies was observed and recorded. The results were classified into three types of haemolysis: α-haemolysis, characterized by partial hydrolysis and the formation of green zones around the colonies; β-haemolysis, which showed complete hydrolysis with clear zones around the colonies; and γ-haemolysis, where no change in the medium occurred, indicating no hydrolysis.

2.6 Molecular analysis

The genomic DNA of the pure bacterial isolate was extracted. A single colony of the bacteria was suspended in 20 µL of TE buffer (Tris EDTA) and processed in a thermo cycler at 95 °C for 10 min. At 6000 rpm for (2–3 min), the sample was centrifuged, and the resulting supernatant was used as a DNA template. The 16S rRNA present in the extracted template DNA was then amplified. Polymerase chain reaction (PCR) was carried out by using universal reverse and forward primers, namely, 1492R (50- GGCTACCTTGTTACGA-30) and 27F (50 -GAGTTTGATCCTGGCTCAG-30). Conditions for PCR were set as follows: Initial denaturation at 94 °C for 2 min followed by thirty cycles of denaturation at 94 °C for 1 min, annealing at 50 °C for 1 min, followed by extension at 72 °C for 1.5 min and the final extension at 72 °C for 5 min. After the completion of PCR, the amplified PCR products were sent for 16S rRNA sequencing through a commercial sequencing service of Invent Dhaka, Bangladesh. The homology of the 16S rRNA gene sequences was checked with the 16S rRNA gene sequences of other organisms using the BLASTN (http://www.ncbi.nih.gov/BLAST) algorithm. The phylogenetic tree was constructed through NCBI BLAST.

2.7 Determination of paraquat degradation using HPLC

To ascertain the amount of paraquat in the bacterial culture, a needed amount of (276 g/L) paraquat was added to 100 mL of the bacterial culture. Before placing the bacterial culture with paraquat into the shaker to promote bacterial growth, 3 mL of culture was removed from the conical flask for OD measurement at 0 hours, with the specified wavelength being 290 nm. This sample was preserved in the refrigerator. Similarly, a 3 ml sample was extracted after 24 hours and 48 hours of incubation. The samples from various shaking hours were then prepared for HPLC analysis. A 10 µL aliquot sample was injected into the XTerraP18 chromatography column (150 mm x 4.6 mm). Triethylamine-phosphate buffer solution (approximately pH 2) and sodium heptane-acetonitrile-water (1.82 g/50 mL/450 mL) were used as the mobile phase. The flow rate was set at 1 ml/min with a column temperature of 25 °C (room temperature). The peak was detected at 290 nm. The sample ran completely for 20 minutes, but the separation was completed within 7.5 minutes.

2.8 In-silico analysis

2.8.1 Preparation of ligand and proteins

The PubChem database was used to retrieve the three-dimensional structure of paraquat [13]. The three-dimensional structures of enzymes involved in the degradation of the herbicide paraquat by *Rhizobium* sp. were retrieved from the Protein Data Bank [14]. Five enzymes-Dehydrogenase, Nitrogenase, Nitrate Reductase, Glutamate Dehydrogenase, and Malate Dehydrogenase were chosen for their close association with the paraquat degradation pathway. Using Pymol, the structure's water and heteroatoms were cleansed. In order to create images of biomolecular structures, PyMOL is frequently utilized [15].

2.8.2 Molecular docking

Molecular docking of all identified compounds in the bacteria was performed using the AutoDock Vina software. The ligands were converted into PDBQT format, and the grid box center and size were set to (X: 50.33 Å, Y: 67.27 Å, Z: 59.25 Å) and (X: 26.29 Å, Y: 12.60 Å, Z: 58.94 Å), respectively [16–18]. The exhaustiveness was set to 8, with the total number of steps, update steps, and energy difference for the ligands adjusted to 200, 1, and 0.1, respectively, using the universal force

field and conjugate gradient algorithms. Docking was performed with PyRx (version 0.8), while Discovery Studio (version 3.0) [19] and PyMOL (version 2.3) [20] were used for analyzing binding interactions.

3. Results

3.1 Physiological characterization

To determine the optimum temperature and pH at which bacteria could degrade paraquat effectively, different temperatures (25°C, 30°C, 37°C, and 40°C) and pH levels (2, 3, 4, 6, 7) were used. From the study, we found that the isolate *Rhizobium* sp. can effectively degrade paraquat at pH 4 and a temperature of 30°C **(Table 1)**. The goal of the optimization was to establish the most favorable conditions for degradation through the isolated bacterium.

Table 1: Role of pH on degradation of paraquat by isolated bacterium. Data was recorded at 290nm.

pH	0 hour	24 hours	48 hours	72 hours
2	0.803±0.006	0.780±0.004	0.774±0.001	0.651±0.007
3	0.794±0.005	0.747±0.002	0.739 ±0.004	0.597±0.002
4	0.78±0.002	0.710±0.005	0.656±0.030	0.539±0.001
5	0.844±0.003	0.787±0.003	0.731 ±0.001	0.573±0.003
6	0.858±0.002	0.806±0.011	0.741±0.002	0.68 ±0.005
7	0.890±0.003	0.806±0.011	0.759± 0.004	0.694±0.005

3.2 Biochemical characterization

3.2.1 Congo red test

Biochemical tests of the isolate were done using Congo red test, and the result was positive.

3.2.2 Heavy metal resistant profile

In the heavy metal resistance test, the isolated bacterium showed resistance to Cd, Pb, Cu, As, and it showed susceptibility to Hg **(Table 2)**.

Table 2: Heavy metal resistant profile of isolated bacterium.

Heavy metal	Cd	Pb	Cu	As	Hg
Concentration (mM)	2	2	2	2	2
	4	4	4	4	4
	6	6	6	6	6
	8	8	8	8	8
	10	10	10	10	10
Result	R	R	R	R	S

3.2.3 Salt tolerance

The isolated bacterium showed a positive result in the salt tolerance test. It was capable of growing in the 2% salt-enriched agar media **(Figure 1)**.

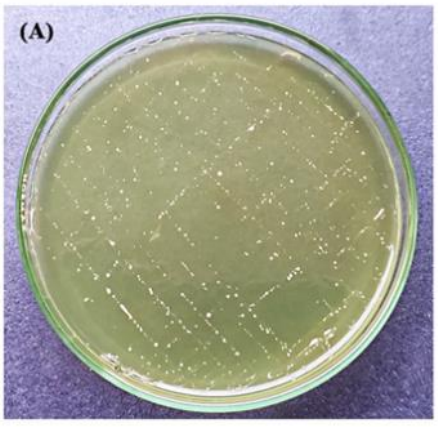

Figure 1: Salt tolerance test of isolated bacterium

Figure 2: Hemolytic test of isolated bacterium.

3.2.4 Antioxidant capacity of intact cells

The result of the antioxidant test shows a positive result. The isolated bacterium can produce antioxidants at nearly 50%. Calculations for each strain and the equation are shown below. Scavenging rate (%) = [1-(Asample-Ablank)/Acontrol] ×100% 1. Scavenging rate of SNKUII (%) = [1-(0.396-0)/0.282]X100% = -40.4% 2. Scavenging rate of SNKUI (%) = [1-(0.143-0)/0.282]X100% = 49.3%.

3.2.5 Blood agar test

In the blood agar test, it indicated that gamma hemolysis occurred. Gamma hemolysis is the third type of hemolytic reaction. It refers to the non-destruction of red blood cells, which is due to the absence of hemolysin. Organisms do not produce hemolysin enzymes that are essential for the breakdown of red blood cells **(Figure 2)**.

3.2.5 Antibiotic sensitivity test

In this research, nine antibiotic discs (penicillin, amoxicillin, gentamicin, ciprofloxacin, ampicillin, kanamycin, chloramphenicol, doxycycline, and erythromycin) were used to test the antibiotic sensitivity of the isolated bacterium. The result showed that the bacterium was susceptible to gentamicin, ciprofloxacin, chloramphenicol, and doxycycline, and resistant to penicillin, amoxicillin, ampicillin, kanamycin, and erythromycin.

3.3 Molecular identification

To identify the isolated paraquat-degrading bacterium, the 16S rRNA gene of the strain was amplified by PCR and sequenced. After gene sequencing and editing of the sequence, it was checked against16S rRNA gene of other organisms that had already been submitted to the NCBI GenBank database. Several sequences were found for the isolate and it showed 98% similarity with *Rhizobium* sp. strain HRI101-4.

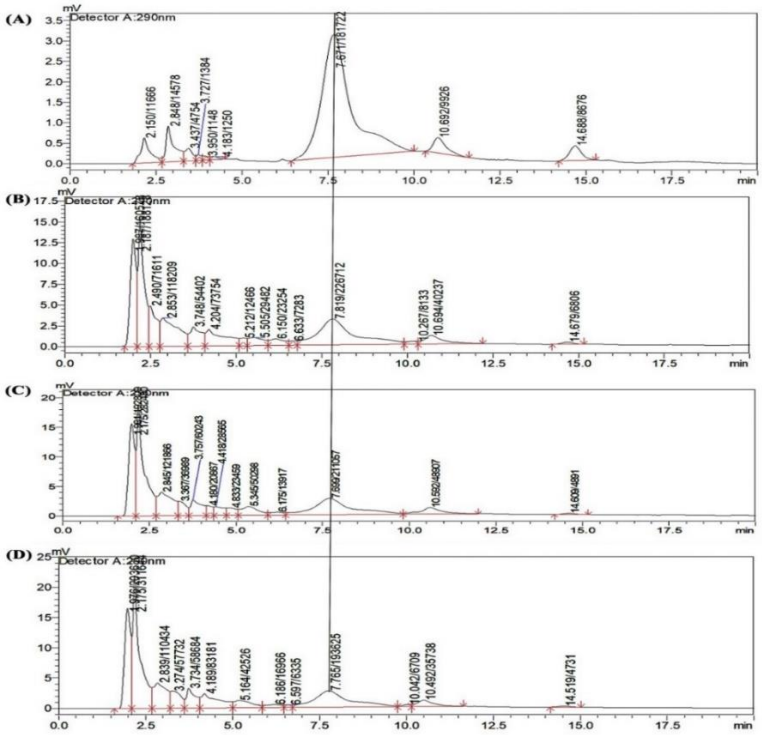

Figure 3: Quantification of the degradation rate of paraquat using reverse-phase high performance liquid chromatography (RP-HPLC). Chromatogram of RP-HPLC for the detection of paraquat absorbance at 0 hour to 48 hours compared with the Standard Tech Grade. The x-axis shows the time and y-axis shows the absorbance intensity at 290nm. Here, A indicates standard, B indicates 0-hour, C indicates 24 hours and D indicates 48 hours sample.

3.4 HPLC quantification of the degradation rate by the isolated bacteria

Several chromatographic methods have been used worldwide to detect the pesticide degradation efficiency of bacteria. Here HPLC has been used to determine the quantity of paraquat. For this reason, standard paraquat (99% pure) was run in the RP-HPLC and the peak of the herbicide was detected at 7.5 min, indicating that it indicated that the retention time is 7.5 min. Later, a preserved sample from Day 0 to Day 3 shaking was run through a column in an RP-HPLC. Three different samples (0 hours, 24 hours and 48 hours) were compared to the standard sample. The standard sample gave the highest peak at 7.5 min, and gradually the peak became lower with the increasing time of incubation **(Figure 3)** indicating the regular degradation of paraquat by the isolated bacterium.

3.5 Molecular docking study

A molecular docking analysis was performed to examine the binding interactions between paraquat and five enzymes from *Rhizobium* sp. The docking score for paraquat with dehydrogenase was -7.3, where paraquat established seven hydrophobic interactions at THR:17, ASP:32, VAL:163, LYS:33, VAL:133, and ASP:176 (twice) positions [**Table 3 and Figure 4 (A, B, C)**]. For nitrogenase, the docking score was -6.5, with paraquat forming eight hydrophobic bonds at ALA: 460 (three times), ALA: 457, TYR: 464, ARG: 425, ILE: 421, and GLU: 463 positions [**Table 3 and Figure 4 (D, E, F)**]. In the case of glutamate dehydrogenase, the docking score was -6.0, and paraquat created seven hydrophobic bonds at ASP:355, LEU:356, THR:166, VAL:167 (twice), and PRO:136 (twice) positions [**Table 3 and Figure 4 (G, H, I**)]. The docking score for nitrate reductase was -5.9, where paraquat formed six hydrophobic bonds at ALA: 452, GLU: 68, LEU: 71, VAL: 451 (twice), and PRO: 70 positions [**Table 3 and Figure 4 (J, K, L)**]. Lastly, for malate dehydrogenase, the docking score was -5.2, with paraquat forming five hydrophobic interactions at THR: 77, VAL: 13 (twice), HIS: 175, and ASN:120 positions [**Table 3 and Figure 4 (M, N, O)**].

Table 3: Non-covalent connections of paraquat and enzymes of *Rhizobium* sp. as well as their binding connections by hydrophobic bond. The relationship distance was calculated in Å.

Ligand	Protein	Amino acid residues	Bond types	Distance (Å)	Docking score (Kcal/mole)
Paraquat (CID_15939)	Dehydrogenase	THR:171	Hydrophobic	3.14	-7.3
		ASP:32	Hydrophobic	3.41	
		VAL:163	Hydrophobic	3.57	
		LYS:33	Hydrophobic	4.43	
		VAL:133	Hydrophobic	3.55	
		ASP:176	Hydrophobic	3.76	
		ASP:176	Hydrophobic	3.47	
Paraquat (CID_15939)	Nitrogenase	ALA:460	Hydrophobic	4.85	-6.5
		ALA:457	Hydrophobic	3.83	
		ALA:460	Hydrophobic	4.51	
		ALA:460	Hydrophobic	5.03	
		TYR:464	Hydrophobic	4.39	
		ARG:425	Hydrophobic	4.48	
		ILE:421	Hydrophobic	3.68	
		GLU:463	Hydrophobic	3.03	
Paraquat (CID_15939)	Glutamate dehydrogenase	ASP:355	Hydrophobic	3.50	-6.0
		LEU:356	Hydrophobic	3.69	
		THR:166	Hydrophobic	3.54	
		VAL:167	Hydrophobic	4.60	
		VAL:167	Hydrophobic	4.99	
		PRO:136	Hydrophobic	5.28	
		PRO:136	Hydrophobic	4.14	
Paraquat (CID_15939)	Nitrate reductase	ALA:452	Hydrophobic	5.18	-5.9
		GLU:68	Hydrophobic	3.73	
		LEU:71	Hydrophobic	4.59	
		VAL:451	Hydrophobic	3.96	
		VAL:451	Hydrophobic	3.90	
		PRO:70	Hydrophobic	5.47	
Paraquat (CID_15939)	Malate dehydrogenase	THR:77	Hydrophobic	3.33	-5.2
		VAL:13	Hydrophobic	3.70	
		VAL:13	Hydrophobic	5.33	
		HIS:175	Hydrophobic	3.57	
		ASN:120	Hydrophobic	3.51	

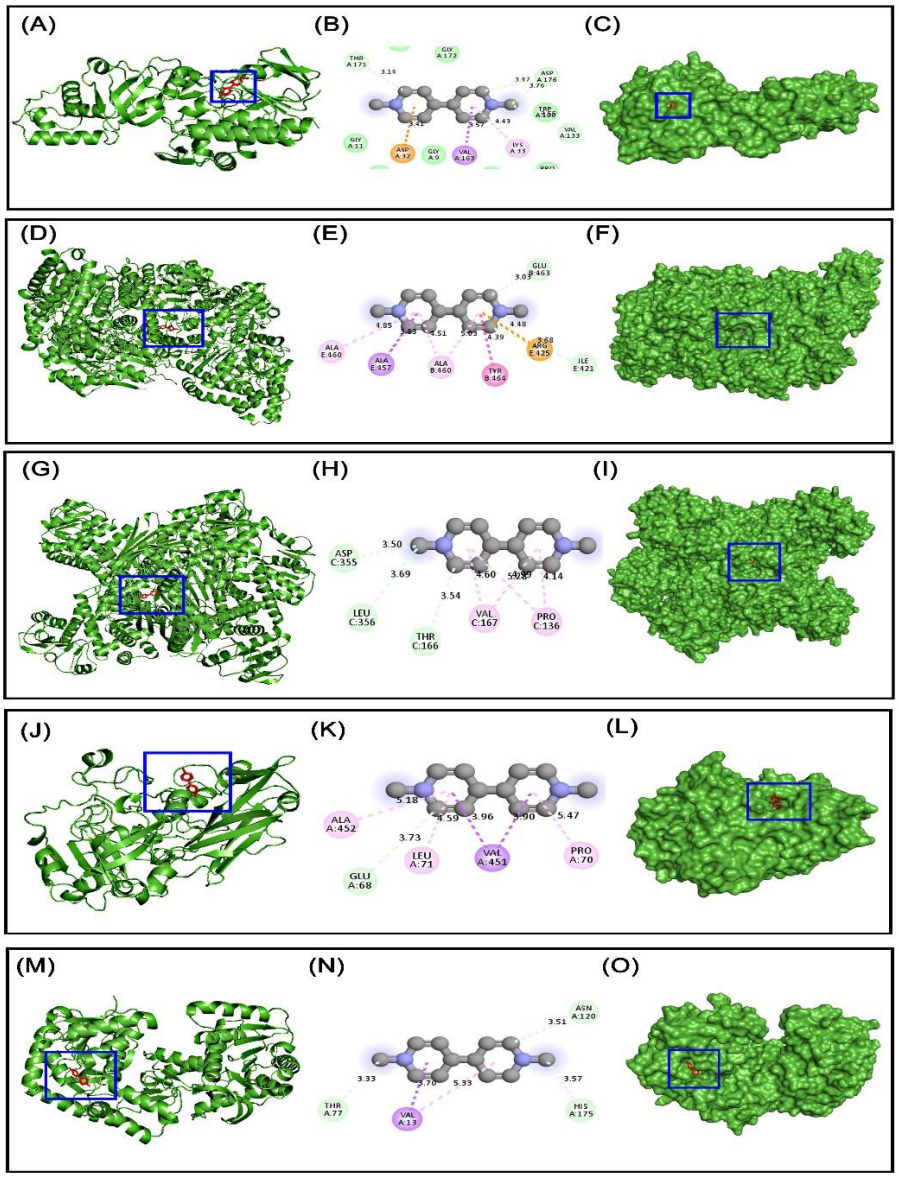

Figure 4: The molecular docking analysis of paraquat with enzymes from *Rhizobium* sp. is presented. Here, A, B, and C illustrate the Cartoon view, 2D view, and surface view of paraquat interacting with the dehydrogenase enzyme, respectively. Similarly, D, E, and F show the Cartoon view, 2D view, and surface view of paraquat with the nitrogenase enzyme. G, H, and I depict the Cartoon, 2D, and surface views of paraquat binding with the glutamate dehydrogenase enzyme. K, and L correspond to the Cartoon, 2D, and surface views of paraquat docking with the nitrate reductase enzyme. Finally, M, N, and O show the Cartoon, 2D, and surface views for paraquat's interaction with the malate dehydrogenase enzyme.

4. Discussion

The widespread application of herbicides paraquat in agriculture has raised significant environmental concerns due to its persistence in soil and potential toxicity to living organisms [21,22]. This study explores the capability of *Rhizobium* sp. strain HRI101-4 to degrade paraquat through in vitro and in silico analyses, providing insights into its potential for sustainable agricultural practices.

The isolation and identification of *Rhizobium* sp. HRI101-4 from Aroxan-treated soils underline the adaptive responses of soil microorganisms to agrochemical stress. The strain demonstrated efficient paraquat degradation, reducing the concentration by 99% under optimized conditions (pH 4, 30°C), as quantified through HPLC analysis. This aligns with previous studies where bacterial strains such as *Pseudomonas putida* and *Enterobacter cloacae* exhibited significant herbicide-degrading capabilities [22,23]. The optimization of environmental parameters in this study corroborates the critical role of pH and temperature in enhancing microbial degradation efficiency [24]. The enzymatic activity, along with the observed

substrate specificity, strongly indicates the involvement of key metabolic pathways dedicated to the breakdown of complex compounds. These findings align with previous studies that underscore the role of microbial enzymatic systems in degrading structurally similar pollutants [25,26]. The observed degradation efficiency suggests that the strain harbors enzymes capable of targeting specific bonds within the substrate, contributing to its rapid breakdown.

The physiological resilience of *Rhizobium* sp. HRI101-4, including its tolerance to salt, heavy metals (Pb, Cd, Cu, As), and acidic conditions, positions it as a robust candidate for field applications in diverse agroecological zones. These findings are consistent with earlier reports that highlight the importance of such traits in microbial bioremediation strategies [27]. The strain's ability to produce antioxidants further supports its adaptation to oxidative stress induced by paraquat, as documented in studies on antioxidant-producing bacteria in contaminated environments [7].

The molecular docking analysis provided mechanistic insights into the degradation process. Key enzymes, including dehydrogenase and nitrogenase, exhibited strong binding affinities with paraquat, as evidenced by docking scores ranging from -7.3 to -5.2 kcal/mol. These interactions involve hydrophobic bonding and stabilize the enzyme-substrate complexes, suggesting specific pathways for paraquat degradation. Similar findings have been reported in enzymatic studies on pollutant degradation, where oxidoreductive enzymes catalyze the breakdown of complex compounds [26,28].

The dual role of *Rhizobium sp.* as a nitrogen-fixing bacterium and a herbicide degrader highlights its potential for sustainable agriculture. By mitigating paraquat residues, this strain not only reduces environmental toxicity but also supports soil fertility, which is crucial for crop productivity. This is particularly relevant in regions like Bangladesh, where paraquat is extensively used, leading to severe environmental pollution [6]. Despite promising results, this study has limitations. The degradation pathway of paraquat was inferred through molecular docking without direct experimental validation of intermediate metabolites. Future studies should include metabolomic profiling to elucidate the complete degradation pathway. Additionally, field trials are necessary to evaluate the strain's performance under real-world conditions and its impact on native soil microbiota.

5. Conclusion

To understand the plausible mRNA expression, prognosis, and mutational effects on the development of different types of cancer regarding NF1, we combined multiple bioinformatics approaches to explore the role of NF1 in cancer development. This study revealed that lower expressions of NF1 were observed specially in BRCA and KIRC. The lower expression of NF1 may be responsible for the higher mutation trend in NF1. These expression patterns of the NF1 gene in cancer cells impact cancer progression across different ethnicities, gender, and cancer stages along with methylation patterns. Additionally, network pharmacology and NF1-related pathway analysis demonstrates it signaling role as well as tumor progression due to the abnormal signaling of NF1. Therefore, the immune infiltrations in BRCA, LUAD, KIRC, and LIHC were also explored for six different cell types. Overall, the findings of this study will further assist researchers to assess invasive mechanisms, tumor development, and therapeutic drug discovery for cancer patients.

Data Availability Statement: The raw data of this manuscript will be made available by the authors.

Conflicts of Interest: There are no potential conflicts of interest.

Funding: Authors received no funding from an external source.

References

[1] A. Sudhakar, "History of Cancer, Ancient and Modern Treatment Methods," *J. Cancer Sci. Ther.*, vol. 01, no. 02, pp. i–iv, 2009, doi: 10.4172/1948-5956.100000e2.

[2] R. L. Siegel, K. D. Miller, H. E. Fuchs, and A. Jemal, "Cancer Statistics, 2021," *CA. Cancer J. Clin.*, vol. 71, no. 1, pp. 7–33, 2021, doi: 10.3322/caac.21654.

[3] H. Sung *et al.*, "Global Cancer Statistics 2020: GLOBOCAN Estimates of Incidence and Mortality Worldwide for 36 Cancers in 185 Countries," *CA. Cancer J. Clin.*, vol. 71, no. 3, pp. 209–249, 2021, doi: 10.3322/caac.21660.

[4] M. Shipitsin and K. Polyak, "The cancer stem cell hypothesis: In search of definitions, markers, and relevance," *Lab. Investig.*, vol. 88, no. 5, pp. 459–463, 2008, doi: 10.1038/labinvest.2008.14.

[5] C. Mattiuzzi and G. Lippi, "Current cancer epidemiology," *J. Epidemiol. Glob. Health*, vol. 9, no. 4, pp. 217–222, 2019, doi: 10.2991/jegh.k.191008.001.

[6] W. E. Gutteridge, "Existing chemotherapy and its limitations," *Br. Med. Bull.*, vol. 41, no. 2, pp. 162–168, 1985, doi: 10.1093/oxfordjournals.bmb.a072044.

[7] M. M. Gottesman, "Mechanisms of cancer drug resistance," *Annu. Rev. Med.*, vol. 53, pp. 615–627, 2002, doi: 10.1146/annurev.med.53.082901.103929.
[8] R. M. Cawthon *et al.*, "A major segment of the neurofibromatosis type 1 gene: cDNA sequence, genomic structure, and point mutations," *Cell*, vol. 62, no. 1, pp. 193–201, 1990, doi: 10.1016/0092-8674(90)90253-B.
[9] Y. Li *et al.*, "Genomic organization of the neurofibromatosis 1 gene (NF1)," *Genomics*, vol. 25, no. 1, pp. 9–18, 1995, doi: 10.1016/0888-7543(95)80104-T.
[10] M. Kiuru and K. J. Busam, "The NF1 gene in tumor syndromes and melanoma," *Lab. Investig.*, vol. 97, no. 2, pp. 146–157, 2017, doi: 10.1038/labinvest.2016.142.
[11] G. Xu *et al.*, "The catalytic domain of the neurofibromatosis type 1 gene product stimulates ras GTPase and complements ira mutants of S. cerevisiae," *Cell*, vol. 63, no. 4, pp. 835–841, 1990, doi: 10.1016/0092-8674(90)90149-9.
[12] M. Bergoug, M. Doudeau, F. Godin, C. Mosrin, B. Vallée, and H. Bénédetti, "Neurofibromin Structure, Functions and Regulation," *Cells*, vol. 9, no. 11, pp. 1–33, 2020, doi: 10.3390/cells9112365.
[13] N. Ratner and S. J. Miller, "A RASopathy gene commonly mutated in cancer: The neurofibromatosis type 1 tumour suppressor," *Nat. Rev. Cancer*, vol. 15, no. 5, pp. 290–301, 2015, doi: 10.1038/nrc3911.
[14] L. Ding *et al.*, "Somatic mutations affect key pathways in lung adenocarcinoma," *Nature*, vol. 455, no. 7216, pp. 1069–1075, 2008, doi: 10.1038/nature07423.
[15] T. Cancer and G. Atlas, "Integrated Genomic Analyses of Ovarian Carcinoma The Cancer Genome Atlas Research Network," *Nature*, vol. 474, no. 7353, pp. 609–615, 2011, doi: 10.1038/nature10166.Integrated.
[16] F. Meric-Bernstam *et al.*, "Concordance of genomic alterations between primary and recurrent breast cancer," *Mol. Cancer Ther.*, vol. 13, no. 5, pp. 1382–1389, 2014, doi: 10.1158/1535-7163.MCT-13-0482.
[17] J. P. Landry *et al.*, "Comparison of Cancer Prevalence in Patients with Neurofibromatosis Type 1 at an Academic Cancer Center vs in the General Population from 1985 to 2020," *JAMA Netw. Open*, vol. 4, no. 3, pp. 1–15, 2021, doi: 10.1001/jamanetworkopen.2021.0945.
[18] R. J. Sullivan, "The role of mitogen-activated protein targeting in melanoma beyond BRAFV600.," *Curr. Opin. Oncol.*, vol. 28, no. 2, pp. 185–191, Mar. 2016, doi: 10.1097/CCO.0000000000000271.
[19] L. Larribère and J. Utikal, "Multiple roles of NF1 in the melanocyte lineage," *Pigment Cell Melanoma Res.*, vol. 29, no. 4, pp. 417–425, 2016, doi: 10.1111/pcmr.12488.
[20] N. M. Warrington *et al.*, "The cyclic AMP pathway is a sex-specific modifier of glioma risk in type I neurofibromatosis patients," *Cancer Res.*, vol. 75, no. 1, pp. 16–21, 2015, doi: 10.1158/0008-5472.CAN-14-1891.
[21] E. Pasmant *et al.*, "SPRED1 disorder and predisposition to leukemia in children," *Blood*, vol. 114, no. 5, p. 1131, 2009, doi: 10.1182/blood-2009-04-218503.
[22] E. Cerami *et al.*, "The cBio Cancer Genomics Portal: An open platform for exploring multidimensional cancer genomics data," *Cancer Discov.*, vol. 2, no. 5, pp. 401–404, 2012, doi: 10.1158/2159-8290.CD-12-0095.
[23] B. Campos *et al.*, "Germline mutations in NF1 and BRCA1 in a family with neurofibromatosis type 1 and early-onset breast cancer," *Breast Cancer Res. Treat.*, vol. 139, no. 2, pp. 597–602, 2013, doi: 10.1007/s10549-013-2538-6.
[24] Y. Murayama *et al.*, "T1 breast cancer associated with von Recklinghausen's neurofibromatosis," *Breast Cancer*, vol. 6, no. 3, pp. 227–230, 1999, doi: 10.1007/BF02967173.
[25] M. Nakamura, A. Tangoku, H. Kusanagi, M. Oka, and T. Suzuki, "Breast cancer associated with Recklinghausen's disease: report of a case.," *Nihon Geka Hokan.*, vol. 67, no. 1, pp. 3–9, Mar. 1998.
[26] A. J. Redig *et al.*, "Clinical and molecular characteristics of NF1-mutant lung cancer," *Clin. Cancer Res.*, vol. 22, no. 13, pp. 3148–3156, 2016, doi: 10.1158/1078-0432.CCR-15-2377.
[27] G. Bollag *et al.*, "Loss of NF1 results in activation of the Ras signaling pathway and leads to aberrant growth in haematopoietic cells," *Nat. Genet.*, vol. 12, no. 2, pp. 144–148, 1996, doi: 10.1038/ng0296-144.
[28] D. F. Calvisi *et al.*, "Inactivation of Ras GTPase-activating proteins promotes unrestrained activity of wild-type Ras in human liver cancer," *J. Hepatol.*, vol. 54, no. 2, pp. 311–319, 2011, doi: 10.1016/j.jhep.2010.06.036.
[29] W. M. Linehan, M. M. Walther, and B. Zbar, "The genetic basis of cancer of the kidney," *J. Urol.*, vol. 170, no. 6 I, pp. 2163–2172, 2003, doi: 10.1097/01.ju.0000096060.92397.ed.
[30] C. M. Johannessen *et al.*, "TORC1 Is Essential for NF1-Associated Malignancies," *Curr. Biol.*, vol. 18, no. 1, pp. 56–62, 2008, doi: 10.1016/j.cub.2007.11.066.
[31] M. Tyers and R. Rottapel, "VHL: A very hip ligase," *Proc. Natl. Acad. Sci. U. S. A.*, vol. 96, no. 22, pp. 12230–12232, 1999, doi: 10.1073/pnas.96.22.12230.

[32] M. Ohh *et al.*, "Ubiquitination of HIF requires direct binding to the beta-domain of the vHL protein," *Nat Cell Biol*, vol. 2, no. 7, pp. 423–427, 2000.
[33] C. C. Hudson *et al.*, "Regulation of Hypoxia-Inducible Factor 1α Expression and Function by the Mammalian Target of Rapamycin," *Mol. Cell. Biol.*, vol. 22, no. 20, pp. 7004–7014, 2002, doi: 10.1128/mcb.22.20.7004-7014.2002.
[34] T. Zefang, K. Boxi, L. Chenwei, C. Tianxiang, and Z. Zemin, "GEPIA2: an enhanced web server for large-scale expression profiling and interactive analysis," *Nucleic Acids Res.*, no. W1, p. W1, 2019.
[35] S. J. Park, B. H. Yoon, S. K. Kim, and S. Y. Kim, "GENT2: An updated gene expression database for normal and tumor tissues," *BMC Med. Genomics*, 2019, doi: 10.1186/s12920-019-0514-7.
[36] D. S. Chandrashekar *et al.*, "UALCAN: A Portal for Facilitating Tumor Subgroup Gene Expression and Survival Analyses," *Neoplasia (United States)*, vol. 19, no. 8, pp. 649–658, 2017, doi: 10.1016/j.neo.2017.05.002.
[37] A. Digre and C. Lindskog, "The Human Protein Atlas—Spatial localization of the human proteome in health and disease," *Protein Sci.*, 2021, doi: 10.1002/pro.3987.
[38] K. Klonowska *et al.*, "Oncogenomic portals for the visualization and analysis of genome-wide cancer data," *Oncotarget*, 2016, doi: 10.18632/ONCOTARGET.6128.
[39] P. Wu *et al.*, "Integration and analysis of CPTAC proteomics data in the context of cancer genomics in the CBIOPortal," *Mol. Cell. Proteomics*, 2019, doi: 10.1074/mcp.TIR119.001673.
[40] J. Gao *et al.*, "Integrative analysis of complex cancer genomics and clinical profiles using the cBioPortal," *Sci. Signal.*, vol. 6, no. 269, 2013, doi: 10.1126/scisignal.2004088.
[41] T. Li *et al.*, "TIMER: A web server for comprehensive analysis of tumor-infiltrating immune cells," *Cancer Res.*, vol. 77, no. 21, pp. e108–e110, 2017, doi: 10.1158/0008-5472.CAN-17-0307.
[42] D. Warde-Farley *et al.*, "The GeneMANIA prediction server: Biological network integration for gene prioritization and predicting gene function," *Nucleic Acids Res.*, 2010, doi: 10.1093/nar/gkq537.
[43] K. Zuberi *et al.*, "GeneMANIA prediction server 2013 update.," *Nucleic Acids Res.*, 2013, doi: 10.1093/nar/gkt533.
[44] J. Montojo *et al.*, "GeneMANIA cytoscape plugin: Fast gene function predictions on the desktop," *Bioinformatics*, 2010, doi: 10.1093/bioinformatics/btq562.
[45] E. Y. Chen *et al.*, "Enrichr: Interactive and collaborative HTML5 gene list enrichment analysis tool," *BMC Bioinformatics*, vol. 14, 2013, doi: 10.1186/1471-2105-14-128.
[46] A. Klose *et al.*, "Selective disactivation of neurofibromin GAP activity in neurofibromatosis type 1 (NF1)," *Hum. Mol. Genet.*, vol. 7, no. 8, pp. 1261–1268, 1998, doi: 10.1093/hmg/7.8.1261.
[47] C. P. Kratz, S. Rapisuwon, H. Reed, H. Hasle, and P. S. Rosenberg, "Cancer in Noonan, Costello, cardiofaciocutaneous and LEOPARD syndromes," *Am. J. Med. Genet. Part C Semin. Med. Genet.*, vol. 157, no. 2, pp. 83–89, 2011, doi: 10.1002/ajmg.c.30300.
[48] L. C. Young *et al.*, "Identification of novel isoforms of the EML4-ALK transforming gene in non-small cell lung cancer," *Cancer Res.*, vol. 68, no. 13, pp. 4971–4976, 2008, doi: 10.1158/0008-5472.CAN-07-6158.
[49] K. Rikova *et al.*, "Global Survey of Phosphotyrosine Signaling Identifies Oncogenic Kinases in Lung Cancer," *Cell*, vol. 131, no. 6, pp. 1190–1203, 2007, doi: 10.1016/j.cell.2007.11.025.
[50] G. V Scagliotti, G. Selvaggi, S. Novello, and F. R. Hirsch, "The biology of epidermal growth factor receptor in lung cancer.," *Clin. cancer Res. an Off. J. Am. Assoc. Cancer Res.*, vol. 10, no. 12 Pt 2, pp. 4227s-4232s, Jun. 2004, doi: 10.1158/1078-0432.CCR-040007.
[51] P. H. . J. B. M. . S. C. T. et al Gary, "The New England Journal of Medicine Downloaded from nejm.org on April 1, 2015. For personal use only. No other uses without permission. Copyright © 1990 Massachusetts Medical Society. All rights reserved.," *New English J. Med.*, vol. 323, no. 16, pp. 1120–1123, 1990.
[52] A. Leonetti *et al.*, *BRAF in non-small cell lung cancer (NSCLC): Pickaxing another brick in the wall*, vol. 66. Elsevier Ltd, 2018. doi: 10.1016/j.ctrv.2018.04.006.
[53] L. Bowman *et al.*, "Clinical Characteristics, Treatments, and Concurrent Mutations in Non–Small Cell Lung Cancer Patients With NF1 Mutations," *Clin. Lung Cancer*, vol. 22, no. 1, pp. 32-41.e1, 2021, doi: 10.1016/j.cllc.2020.09.011.
[54] Ş. Güran and M. Safali, "A case of neurofibromatosis and breast cancer: Loss of heterozygosity of NF1 in breast cancer," *Cancer Genet. Cytogenet.*, vol. 156, no. 1, pp. 86–88, 2005, doi: 10.1016/j.cancergencyto.2004.04.019.
[55] H. Ogata, H. Sato, J. Takatsuka, and L. M. De Luca, "Human breast cancer MDA-MB-231 cells fail to express the neurofibromin protein, lack its type I mRNA isoform and show accumulation of P-MAPK and activated Ras," *Cancer Lett.*, vol. 172, no. 2, pp. 159–164, 2001, doi: 10.1016/S0304-3835(01)00648-6.

[56] K. M. Shannon *et al.*, "Loss of the normal NF1 allele from the bone marrow of children with type 1 neurofibromatosis and malignant myeloid disorders.," *N. Engl. J. Med.*, vol. 330, no. 9, pp. 597–601, Mar. 1994, doi: 10.1056/NEJM199403033300903.
[57] A. Bernards and J. Settleman, "GAPs in growth factor signalling," *Growth Factors*, vol. 23, no. 2, pp. 143–149, 2005, doi: 10.1080/08977190500130480.
[58] F. Latif *et al.*, "Identification of the von Hippel-Lindau disease tumor suppressor gene," *Science (80-.).*, vol. 260, no. 5112, pp. 1317–1320, 1993, doi: 10.1126/science.8493574.
[59] J. R. Gnarra *et al.*, "Mutations of the VHL tumour suppressor gene in renal carcinoma," *Nat. Genet.*, vol. 7, no. 1, pp. 85–90, 1994, doi: 10.1038/ng0594-85.
[60] I. Eisenbarth, K. Beyer, W. Krone, and G. Assum, "Toward a survey of somatic mutation of the NF1 gene in benign neurofibromas of patients with neurofibromatosis type 1," *Am. J. Hum. Genet.*, vol. 66, no. 2, pp. 393–401, 2000, doi: 10.1086/302747.
[61] S. A. Rasmussen *et al.*, "Chromosome 17 loss-of-heterozygosity studies in benign and malignant tumors in neurofibromatosis type 1," *Genes, Chromosom. Cancer*, vol. 28, no. 4, pp. 425–431, 2000, doi: 10.1002/1098-2264(200008)28:4<425::aid-gcc8>3.3.co;2-5.
[62] A. M. John, M. Ruggieri, R. Ferner, and M. Upadhyaya, "A search for evidence of somatic mutations in the NF1 gene," *J. Med. Genet.*, vol. 37, no. 1, pp. 44–49, 2000, doi: 10.1136/jmg.37.1.44.